

Journal of Experimental Botany, Vol. 76, No. 18 pp. 5465–5480, 2025 https://doi.org/10.1093/jxb/eraf270 Advance Access Publication 18 June 2025



## **RESEARCH PAPER**

# Arabidopsis thaliana iron superoxide dismutase FeSOD1 protects ARGONAUTE 1 in a copper-dependent manner

Ariel H. Tomassi<sup>1,†</sup>, D, Ana Perea-García<sup>2,†</sup>, Guillermo Rodrigo<sup>3</sup>, D, Javier Sánchez-Vicente<sup>1</sup>, D, Adriana E. Cisneros<sup>1</sup>, D, Marta Olmos<sup>2</sup>, Amparo Andrés-Bordería<sup>2</sup>, Lucio López-Dolz<sup>1</sup>, D, José-Antonio Daròs<sup>1</sup>, D, Lola Peñarrubia<sup>2,\*</sup>, D, and Alberto Carbonell<sup>1,\*</sup>, D

Received 26 February 2025; Editorial decision 13 June 2025; Accepted 17 June 2025

Editor: Pablo Manavella, Instituto de Hortofruticultura Subtropical y Mediterránea, CSIC, Spain

## **Abstract**

Copper (Cu) deficiency compromises plant growth and limits crop productivity. Plants respond to Cu scarcity by activating the expression of several miRNAs, known as Cu-miRNAs, which degrade mRNAs from various cuproproteins to conserve Cu. Cu-miRNAs, like most plant miRNAs, associate with ARGONAUTE 1 (AGO1), the primary effector protein of miRNA-mediated gene silencing pathways, whose function is typically modulated by interacting proteins acting as cofactors. However, how AGO1 is regulated and functions under Cu deficiency remains unknown. Here, we searched for AGO1 interactors in *Arabidopsis thaliana* plants expressing a functional AGO1 protein tagged with the Twin-Strep-tag (TST) polypeptide, grown under Cu-sufficient or Cu-deficient conditions. TST-AGO1 complexes were affinity purified, and proteins were identified using tandem MS. Interestingly, the iron superoxide dismutase 1 (FeSOD1) encoded by *FSD1* was enriched in TST-AGO1 complexes purified from plants grown under Cu deficiency. Moreover, *fsd1-2* mutant plants showed reduced levels of AGO1 compared with wild-type plants under Cu sufficiency, while both Cu-miRNA-specific and general AGO1 target mRNAs accumulated to higher levels in *fsd1-2* plants under both Cu-deficient and Cu-sufficient conditions compared with wild-type plants. These findings suggest that FeSOD1 is essential for proper AGO1 function, and that its superoxide dismutase activity, which mitigates oxidative stress, enhances AGO1 stability, particularly under Cu deficiency.

<sup>&</sup>lt;sup>1</sup> Instituto de Biología Molecular y Celular de Plantas (Consejo Superior de Investigaciones Científicas-Universitat Politècnica de València), Valencia, Spain

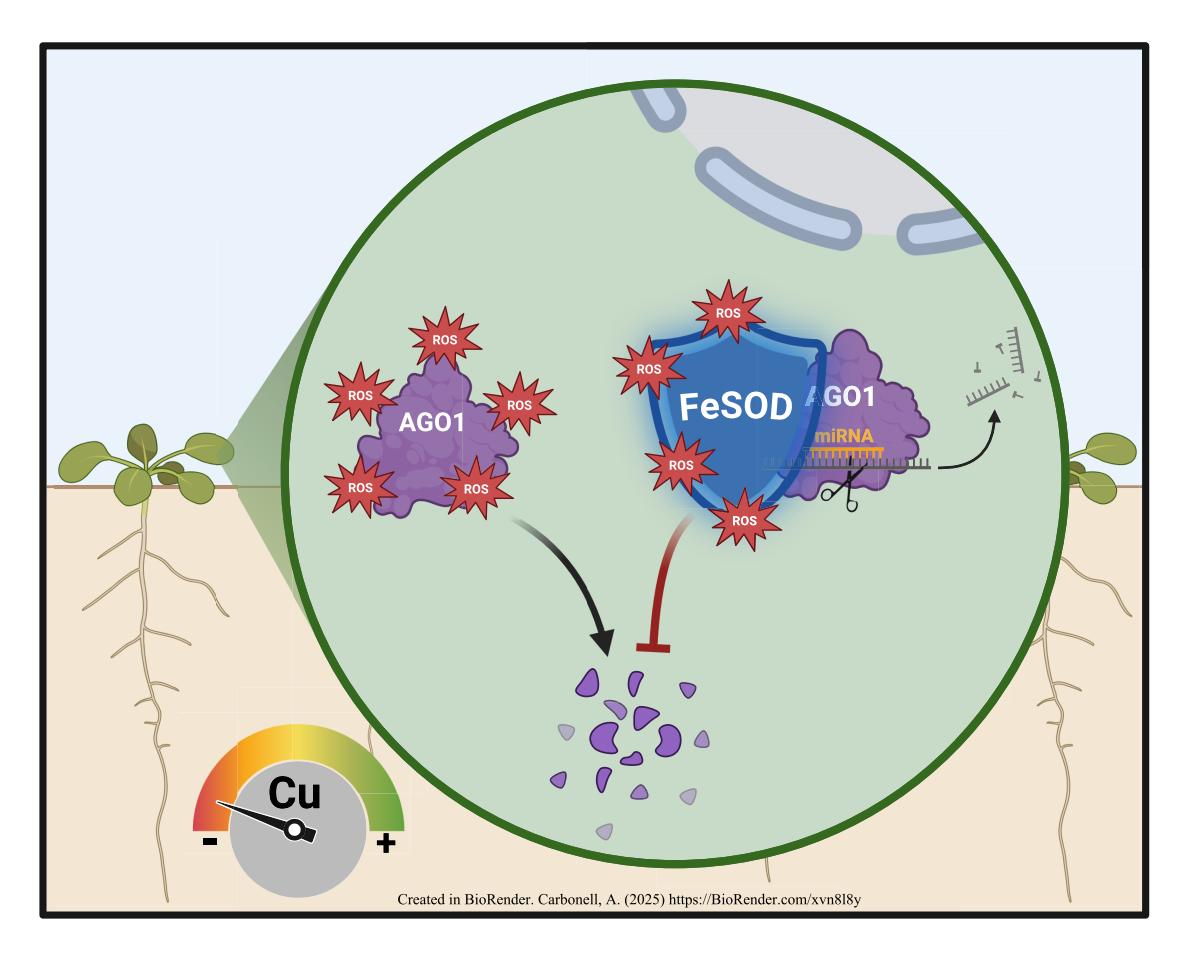
<sup>&</sup>lt;sup>2</sup> Departament de Bioquímica I Biología Molecular, Universitat de València, Burjassot, Valencia, Spain

<sup>&</sup>lt;sup>3</sup> Institute for Integrative Systems Biology (I2SysBio), CSIC-University of Valencia, Paterna 46980, Spain

<sup>\*</sup> Correspondence: Lola.Penarrubia@uv.es or acarbonell@ibmcp.upv.es

<sup>&</sup>lt;sup>†</sup> These authors contributed equally to this work.

## **Graphical abstract**



Keywords: AGO1, AP-MS, Arabidopsis thaliana, copper, FeSOD1, miRNA, TST.

## Introduction

Plants require rapid and flexible responses to changing environmental conditions throughout their developmental stages, particularly under stress. miRNAs are a class of small RNAs (sRNAs) that regulate gene expression post-transcriptionally and function as key players in the interplay between development and stress responses (Borges and Martienssen, 2015; Song et al., 2019). miRNAs regulate a wide range of developmental processes including hypocotyl elongation, root development, and the transition from vegetative to reproductive phases (Schwab et al., 2005; Meng et al., 2010). Conversely, certain miRNAs are integral to stress responses, modulating plant adaptation to a multitude of environmental conditions such as nutrient availability, low temperatures, and drought (Buhtz et al., 2010; Martin et al., 2010; Patel et al., 2017). For instance, miRNAs involved in nutrient stress, including transition metal deficiencies, play significant roles in plant adaptation (Patel et al., 2017) by regulating processes such as metal uptake, chelation, antioxidant response, and hormone signaling (Ding et al., 2020).

The availability of essential transition metals, such as copper (Cu) and iron (Fe), often limits agricultural productivity (Broadley et al., 2012). These metals, essential as cofactors in metalloproteins central to life, can also cause toxicity when in excess, leading to increased reactive oxidative species (ROS) production (Farooq et al., 2019). Due to their dual nature as essential and toxic elements, plants have developed complex homeostatic networks to ensure their uptake and distribution whilepreventing toxicity (Puig and Peñarrubia, 2009; Pilon, 2011; Kobayashi et al., 2019; Kumar et al., 2021).

ROS are also produced under metal scarcity, as the malfunctioning of key redox metalloproteins in respiratory and photosynthetic electron transport chains causes oxidative stress (Shahbaz and Pilon, 2019). Among ROS, the superoxide radical is one of the most harmful species, capable of damaging macromolecules. ROS detoxification involves superoxide dismutases (SODs), which in plants use different metals as cofactors, functioning in various cellular compartments under diverse conditions. Plant SODs include FeSODs, Cu and zinc (Zn)SODs (Cu/ZnSODs), and manganese (Mn) MnSODs (Ravet and Pilon, 2013).

In Arabidopsis thaliana (Arabidopsis), the Cu-miRNAs play crucial roles in plant responses under Cu deficiency, orchestrating metal redistribution and substituting Cu/ZnSODs with FeSODs (Yamasaki et al., 2007; Pilon, 2017). Cu-miRNAs are proposed to modulate metalloprotein mRNAs posttranscriptionally, establishing a metal prioritization hierarchy and preventing interference with metal-sensitive processes (Shahbaz and Pilon, 2019; Perea-García et al., 2022). Cu-miRNAs, including miR397, miR398, miR408, and miR857, are induced under Cu deficiency and primarily target mRNAs encoding Cu/ZnSODs (CSD1 and CSD2), plantacyanin, and laccases (Pilon, 2017). Cu-miRNAs containing cisregulatory domains in their promoters are recognized by a SQUAMOSA BINDING PROTEIN-LIKE (SPL) family member, SPL7, the master transcription factor driving Cu-deficiency responses (Yamasaki et al., 2009; Bernal et al., 2012). In addition to Cu-miRNAs, plasma membrane Cu transporter genes (COPT1, COPT2, and COPT6) as well as FSD1 (encoding FeSOD1) are regulated similarly (Yamasaki et al., 2007; Bernal et al., 2012; Garcia-Molina et al., 2013). These processes enhance high-affinity Cu uptake and metalloprotein substitution as primary responses to nutrient scarcity.

Importantly, SPL7 belongs to a large family of transcription factors mainly involved in the control of developmental phase transitions and reproduction (Huijser and Schmid, 2011). Based on their sizes and similarities, the Arabidopsis SPL family can be grouped in two subfamilies: large SPLs (comprising SPL1, SPL7, SPL12, SPL14, and SPL16) and small SPLs (the remaining 11 SPLs) (Guo et al., 2008; Xing et al., 2010). The small SPLs, with the exception of SPL8, share an miRNA response element that is complementary to miR156 responsive in the timing of the vegetative and reproductive phase transitions (Rhoades et al., 2002; Schwab et al., 2005; Wu and Poethig, 2006; Gandikota et al., 2007). SPL3-overexpressing plants, resistant to miR156 regulation, display a strong reduction in SPL7-mediated Cu-deficiency responses, probably due to competition between SPL7 and miR156-regulated SPL3 for *cis*-element binding in target promoters (Perea-García et al., 2021). Therefore, the balance of miR156 SPL targets and non-targets is essential for SPL7-mediated Cu-deficiency adaptation at different levels, underscoring that the effect of miRNA on its targets could serve to reinforce the miRNA non-target function. Thus,

while Cu-miRNAs function as post-transcriptional modulators of metalloproteins, allowing flexible Cu redistribution, other miRNAs, such as miR156, operate upstream, balancing the relative abundance of SPL transcription factors to integrate Cu-deficiency responses with developmental processes.

ARGONAUTE (AGO) proteins act as the effector proteins in sRNA-mediated RNA silencing pathways in eukaryotes (Meister, 2013). In plants, AGOs regulate essential biological processes such as development, stress responses, genome stability, and defense against pathogens, particularly against viruses (Carbonell and Carrington, 2015; Fang and Qi, 2016; Carbonell, 2017). They associate with sRNAs such as miRNAs and siRNAs to form the RNA-induced silencing complex (RISC), which directs the endonucleolytic cleavage or translational repression of sequence-complementary target RNAs (Huntzinger and Izaurralde, 2011). Arabidopsis has 10 AGO members that have functionally diverged during the specialization of sRNA-based RNA silencing pathways (Chapman and Carrington, 2007). AGO1 is the principal miRNA-associated AGO (Vaucheret et al., 2004) and, consequently, ago 1 mutants show severe growth defects (Morel et al., 2002). AGO1 protein levels are regulated at different transcriptional and post-transcriptional levels (Molinier, 2020). For instance, AGO1 can be ubiquitinated and degraded through the ubiquitin-proteasome pathway that tags AGOs with ubiquitin molecules for their degradation by the 26S proteasome (Earley et al., 2010), or through autophagy by sequestration of AGO1 proteins in autophagosomes (Derrien et al., 2012). In contrast, AGO1 protein is stabilized by its binding to sRNAs (Vaucheret et al., 2006; Hacquard et al., 2022), as unloaded AGO1 is more prone to degradation, by its sequestration into stress granules (Leung et al., 2006) or through its association with cofactors. AGO1 physically interacts with several proteins, including chaperones involved in RISC loading such as HEAT SHOCK PROTEIN 70 (HSP70), HSP90, and CYCLOPHILLIN 40/ SQUINT (CYP40/SQN), which facilitate the conformational opening of AGO1 during sRNA loading (Iki et al., 2010, 2012; Iwasaki et al., 2010). Moreover, TRANSPORTIN 1 (TRN1), ENHANCED MiRNA ACTIVITY 1 (EMA1) β, and CONSTITUTIVE ALTERATIONS IN THE SMALL RNAS PATHWAYS 9 (CARP9) proteins interact with AGO1 to modulate miRNA loading (Wang et al., 2011; Cui et al., 2016; Tomassi et al., 2020), while PROTEIN ARGININE METHYLTRANSFERASE 5 (PRMT5) associates with AGO1 to promote its methylation (Martín-Merchán et al., 2024). Finally, proteins known to interact with AGO1 in response to stress are limited to DAMAGE-SPECIFIC DNA BINDING PROTEIN 2 (DDB2), TUDOR DOMAN-CONTAINING PROTEIN 1 (TSN1) and TSN2, and SWI/SNF complexes in response to UV, general stress, and hormone or cold stress, respectively (Schalk et al., 2017; Liu et al., 2018; Gutierrez-Beltran et al., 2021). However, proteins specifically interacting with AGO1 during the metal stress response have not been identified.

## 5468 | Tomassi et al.

To better understand the role of AGO1 in response to Cu deficiency, we searched for AGO1 interactors in Arabidopsis transgenic lines expressing a functional AGO1 protein tagged with the bidentate polypeptide Twin-Strep-tag (TST), grown under Cu-sufficient or Cu-deficient conditions. AGO1 complexes were affinity purified, and proteins were identified by tandem [affinity purification MS (AP-MS)]. Interestingly, FSD1-encoded FeSOD1, recently proposed as an AGO1 interactor as a result of a yeast two-hybrid screening (Bressendorff et al., 2023), was enriched in AGO1 complexes purified from plants grown under Cu deficiency. fsd1-2 mutant plants accumulated lower levels of AGO1 compared with Col-0 plants under Cu sufficiency, and both Cu-miRNA-specific and general AGO1 target mRNAs accumulated to higher levels in fsd1-2 plants grown under Cu deficiency and sufficiency, respectively, compared with Col-0. These results underscore the role of FeSOD1 in protecting AGO1 stability, especially under Cu deficiency, where its function in miRNA-mediated gene silencing pathways becomes particularly important.

## Materials and methods

Plant materials, growth conditions, and plant phenotyping

ago1-25 is a hypomorphic mutant obtained in an ethyl methanesulfonate (EMS) mutagenesis and described before (Morel et al., 2002). fsd1-2 (GABI\_740E11) is a mutant line derived from a T-DNA insertion and also described before (Melicher et al., 2022). Wild-type Arabidopsis cv Columbia 0 (Col-0), ago1-25, and fsd1-2 seeds were grown on plates where the Cu concentration was 1 mM, considered as Cu sufficiency, as previously described (Perea-García et al., 2020). Seedlings were grown for 10 d under long-day photoperiodic conditions (16 h light, 23 °C/18 h darkness, 16 °C). Root length of 10-day old seedlings was measured using ImageJ (Abramoff et al., 2004). To induce severe Cu deficiency, 100 μM bathocuproine disulfonate (BCS) was added to the growth medium. For cadmium excess assays, the growth medium was supplemented with 30 μM CdCl<sub>2</sub>. Oxidative stress was induced by transferring seedlings, initially grown for 5 d under Cu-sufficiency conditions, to fresh medium supplemented with 2 μM methyl viologen (MV) for an additional 5 d.

#### Transgene constructs

pENTR-pAGO1-3×HA-AGO1 (Carbonell et al., 2012) was digested with HindIII and KpnI, and the two fragments (7812 bp and 1425 bp) were gel-purified. The 1425 bp fragment was ligated into HindIII/ KpnI-digested pBSIIKS+ to generate pBS-pAGO1-3×HA. A 4266 bp linear pBS-pAGO1 fragment lacking the 3×HA tag was amplified using pBS-pAGO1-3×HA as template and oligonucleotide pair D2475/ D2476, gel purified, and assembled with a 136 bp TST-AGO1 fragment using a plasmid containing a TST-GFP (green fluorescent protein) cassette and oligonucleotide pair D2477/2478 in the presence of GeneArt Gibson Assembly HiFi Master Mix (Invitrogen) to generate pBS-pAGO1-TST. pBS-pAGO1-TST was digested with HindIII-KpnI, and the resulting 1437 bp fragment was ligated to the 7812 bp mentioned before, to generate pENTR-pAGO1-TST-AGO1. Finally, the pAGO1-TST-AGO1 cassette was cloned by LR recombination into pMDC99, a Gateway-compatible plant transformation vector (Curtis and Grossniklaus, 2003), to generate pMDC99-pAGO1-TST-AGO1. Nucleotide and amino acid sequences of TST-AGO1 and TST-GFP are listed in Supplementary Dataset S1.

A 6003 bp and an 863 bp fragment was amplified from *pENTR-pAGO1-3*×*HA-AGO1* (Carbonell *et al.*, 2012) and *TST-GFP* plasmid with oligonucleotide pair AC-22/AC-23 and AC-20/AC-21, respectively. Both fragments were assembled in the presence of GeneArt Gibson Assembly HiFi Master Mix (Invitrogen) to generate *pENTR-pAGO1-TST-GFP*. The *pAGO1-TST-GFP* was transferred by LR recombination into *pMDC99* to generate *pMDC99-pAGO1-TST-GFP*.

#### RNA and protein preparation

Total RNA form Arabidopsis seedlings or inflorescences was isolated as before (Cisneros *et al.*, 2023). Triplicate samples from pools of Arabidopsis seedlings or inflorescences were analyzed. Total protein extracts were prepared in 2× PDB buffer (0.0625 M Tris pH 6.8, 2% SDS, 10% glycerol, 10% mercaptoethanol, 0.02% bromophenol blue) in a 1:5 tissue:buffer ratio.

## Real-time quantitative reverse transcription-PCR

cDNA synthesis and quantitative PCR (qPCR) analysis were performed essentially as before (Cisneros et al., 2025). Briefly, 500 ng of DNase I-treated total RNA was used to produce cDNA from 10-day-old Arabidopsis seedlings with the PrimeScript RT Reagent Kit (Perfect Real Time, Takara) according to the manufacturer's instructions. Quantitative reverse transcription-qPCR (RT-qPCR) was done on optical 96-well plates in a QuantStudio 3 Real-Time PCR system (Thermo Fisher Scientific, Waltham, MA, USA) wuth these conditions: 20 s at 95 °C, followed by 40 cycles of 95 °C for 3 s and 60 °C for 30 s, with an additional melt curve stage consisting of 15 s at 95 °C, 1 min at 60 °C, and 15 s at 95 °C. The 20 μl reaction included 10 μl of 2× TB Green Premix Ex Taq (Takara), 2 µl of diluted cDNA (1:5), 0.4 µl of ROX II Reference Dye (50X), and 300 nM of each gene-specific primer. Oligonucleotides used for RT-qPCR are listed in Supplementary Table S1. Target mRNA expression levels were calculated relative to reference genes ACT2 and UBQ10, using the delta delta cycle threshold comparative method of QuantStudio Design and Analysis software, version 1.5.1 (Thermo Fisher Scientific). Three independent biological replicates, and two technical replicates for each biological replicate were analyzed.

## Small RNA blot assays

Small RNA blot assays and band quantification from radioactive membranes were done as described (Cisneros *et al.*, 2022). Oligonucleotides used as probes for sRNA blots are listed in Supplementary Table S1.

## Protein blot assays

Proteins were separated in NuPAGE Novex 4–12% Bis–Tris gels (Invitrogen), transferred to Protran nitrocellulose membranes (Amersham), and detected by chemiluminescence using specific antibodies and SuperSignal West Pico PLUS chemiluminescent substrate (ThermoFisher Scientific) as before (Cisneros et al., 2025). Here, for detection of TST-tagged proteins, StrepMAB-Classic HRP Twin-Strep-Tag antibody (IBA) at a 1:10000 dilution was used. For detection of endogenous AGO1 and HISTONE3 (H3), anti-AGO1 (Agrisera) and anti-histone 3 (Abcam) were used at 1:10000 and 1:4000 dilutions, respectively, and conjugated with a 1:20 000 dilution of goat anti-rabbit IgG horseradish peroxidase (HRP) secondary antibody (ThermoFisher Scientific). Images were acquired with an ImageQuant 800 CCD imager (Cytiva) and analyzed with ImageQuantTL v10.2 (Cytiva). Ponceau red S solution (Thermo Fisher Scientific) staining of membranes was used to verify the global protein content of the samples.

## Hydrogen peroxide quantification

Hydrogen peroxide (H<sub>2</sub>O<sub>2</sub>) levels were determined following the colorimetric method as described (Junglee et al., 2014), with minor modifications. Briefly, 150 mg of frozen tissue from 10-day-old Arabidopsis Col-0 seedlings grown under Cu-sufficiency or Cu-deficiency conditions was homogenized at 4 °C in 1 ml of extraction buffer containing 0.25 ml of 0.1% (w/v) trichloroacetic acid (TCA), 0.5 ml of 1 M potassium iodide (KI), and 0.25 ml of 10 mM potassium phosphate buffer (pH 7.6). Samples and buffers were protected from light throughout the procedure. After centrifugation at 12 000 g for 15 min at 4 °C, 200 µl of the supernatant was transferred to a 96-well microplate and incubated at room temperature in the dark for 20 min. Absorbance was measured at 350 nm using an Infinite® 200 PRO microplate reader (TECAN). H<sub>2</sub>O<sub>2</sub> concentration was calculated using a standard curve prepared with H<sub>2</sub>O<sub>2</sub> solutions diluted in 0.1% TCA. Five biological replicates of at least 20 seedlings per replicate were analyzed per condition, each measured in duplicate (technical replicates).

#### Statistical analysis

Statistical tests are described in the figure legends. Significant differences were determined with two-tailed Student's t-test (P<0.05).

## Affinity purification of protein complexes

Protein complexes containing TST-tagged protein products were purified from 1.5 g of 12-day-old seedlings by affinity chromatography in native conditions using a 1 ml Strep-Tactin XT spin column (IBA) as previously described (Martinez et al., 2016).

## Protein identification by liquid chromatography coupled with tandem mass spectrometry

Protein preparations were separated by SDS-PAGE using 4% and 10% acrylamide for the stacking and resolving gel, respectively. Electrophoresis was stopped when the front entered 1 cm into the resolving gel, and the gel was stained with Coomassie. The bands were cut for subsequent in-gel digestion with trypsin (12.5 ng µl<sup>-1</sup>). The digest was acidified with 0.5% trifluoroacetic acid (TFA) to stop digestion. The peptides were desalted using C18 columns according to the manufacturer's protocol (Pierce C18 Spin Columns, Thermo Scientific). The peptides were dried in a speedvac and resuspended in 15 µl of mobile phase [2%] acetonitrile (ACN), 0.05% TFA] for injection into a HPLC column. The mixture of tryptic peptides was analyzed by high-resolution MS using an Orbitrap Fusion (Thermo Scientific) in 'data dependent acquisition' mode, equipped with a nanoESi ion source. The peptide extract, diluted in 2% ACN and 0.05% TFA, was first separated in an Ultimate 3000 Dionex UHPLC (Thermo Scientific) under the following chromatographic conditions: pre-concentration on a C18 pre-column (PepMap100, 5 μm, 300 μm×5 mm, Thermo Scientific) at a flow rate of 5 µl min<sup>-1</sup> for 3 min in 98% ACN and 0.1% TFA. The chromatographic gradient of 4–40% ACN was applied at a flow rate of 300 nl min<sup>-1</sup> on a C18 nano-column (Acclaim PepMap RSLC 75 µm×50 cm, Thermo Scientific) over 60 min. The total chromatography time was 85 min. The Orbitrap Fusion operated in positive mode with a voltage of 2 kV. The mass range in 'full scan' mode was  $400-1500 \, m/z$  in the Orbitrap at a resolution of 120 000, with an AGC target of 4×10<sup>5</sup> and a dynamic 'injection time'. Peptide analysis was performed in 'data dependent acquisition' mode, operating in MS/MS Top 50 mode, fragmenting as many high-intensity ions as possible per 'full scan' within a cycle time of 3 s. Fragmentation spectra were acquired in the linear trap by collision-induced dissociation (CID) fragmentation at a collision energy of 35%, with a dynamic injection time and an AGC target of  $1 \times 10^2$ . A dynamic exclusion time of 15 s was included for each ion to avoid repetitive ion fragmentation. Protein identification was done using Proteome

Discoverer 2.1 (PD2.1, Thermo Fisher Scientific). Proteins were identified with the following conditions: database, Uniprot\_Arabidopsisthaliana+AGO-sequences; tolerance, 10 ppm for Orbitrap and 0.02 Da for Ion Trap; maximum of 1 missed cleavages; \*b-ions weight 1 (CID) and 0.3 (HCD); \*y-ions weigh: 1 (CID-HCD); dynamic modifications, oxidation (Met); fixed modifications, carbamidomethylation (Cys) (\*depends on the fragmentation type: CID or HCD); acceptance criteria, Percolator (Delta CN<0.05); and false discovery rate (FDR) of 1% against a decoy database. Resulting Excel sheets contain the identifications at the peptide and protein levels (Supplementary Dataset S2). The data included in the report are filtered by a 1% FDR based on the probability values obtained by Percolator. The minimum number of peptides per protein is 1.

#### Computational analysis

A previously developed bioinformatic pipeline (Ambrós et al., 2021) was used to process all information obtained via proteomics. From the raw proteomic lists, all plant proteins were identified and mapped to Arabidopsis genes (proteins), keeping the normalized MS peak area as a quantitative measure. Specifically, we identified proteins from green plants by GenInfo Identifier (GI) through Mascot analysis and conducted sequence alignments using BLAST to identify individual genes in A. thaliana, using data from The Arabidopsis Information Resource (TAIR) version 10 (Lamesch et al., 2012). For each hit, the associated amino acid sequence was retrieved from the NCBI database in FASTA format using the Biopython Entrez module. Only alignments with e-values <0.0001 were considered, and any redundant elements were excluded. The protein list obtained from the Cu-deficiency condition was compared against the list obtained from the Cu-sufficiency condition in a quantitative manner (i.e. by subtracting the MS peak areas) for each transgenic line, discarding those proteins present in control pAGO1-TST-GFP lists for each condition. After the control filtering, if a protein was in one list but not in the other, we considered |log<sub>2</sub> fold|=100 (arbitrary value, denoted by Inf in the figures) positive for proteins detected in Cu deficiency but not in sufficiency and negative for proteins detected in Cu sufficiency but not in deficiency. All genes (proteins) in the lists were functionally annotated according to the information from TAIR10.

#### Gene and virus identifiers

Arabidopsis gene identifiers are: ACT2 (AT3G18780), AGO1 (AT1 G48410), ARF8 (AT5G37020), ARPN (AT2G02850), CCS (AT1G 12520), CSD1 (AT1G08830), CSD2 (AT2G28190), (AT4G25100), GSTU25 (AT1G17180), LAC3 (AT2G30210), MSD1 (AT3G10920) NF-YA9 (AT3G20910), SPL3 (AT2G33810), SPL9 (AT2G42200), TCP4 (AT3G15030), and UBQ10 (AT4G05320).

## Results

Generation and functional characterization of Arabidopsis transgenic lines expressing TST-tagged AGO1

TST is an advanced affinity tag used for the purification and detection of recombinant proteins under non-denaturing, mild conditions (Schmidt et al., 2013). It consists of a tandem arrangement of two Strep-tag II sequences, designed to enhance binding affinity for Strep-Tactin, a derivative of streptavidin. The TST coding sequence was inserted after the AGO1 start codon to tag the N-terminus of AGO1, previously done with HA or FLAG peptides (Baumberger and Baulcombe, 2005; Carbonell et al., 2012), in the pAGO1:TST-AGO1 construct, which includes authentic AGO1 regulatory sequences

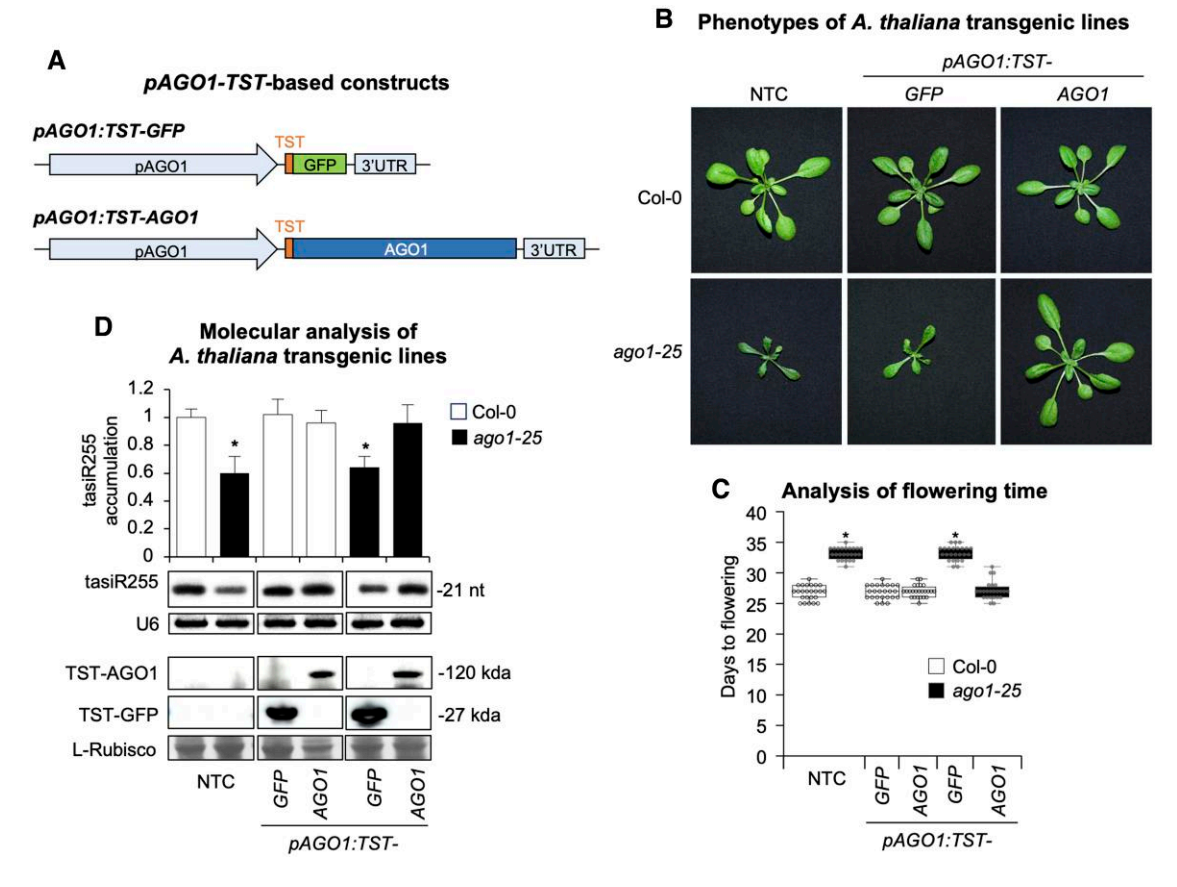


**Fig. 1.** Phenotypic and molecular analyses of Arabidopsis Col-0 and ago1-25 transgenic plants expressing TST-tagged AGO1 or GFP. (A) Diagram of the constructs. TST, GFP, and AGO1 sequences are shown in coloured boxes. The AGO1 endogenous promoter and 3'-untranslated region (UTR) regulatory sequences are also shown in coloured boxes. (B) Pictures of 21-day-old Col-0 (top panel) and ago1-25 (bottom panel)  $T_1$  transgenic plants, homozygous for the transgene. Col-0 and ago1-25 non-transgenic controls (NTCs) are included. (C) Box plot representing the mean flowering time of Col-0 and ago1-25 NTC and  $T_1$  transgenic plants (n=24). Pairwise Student's t-test comparisons are represented with an \* if significantly different (p<0.05) compared with Col-0 NTC. (D) Accumulation of tAS1tC-dependent tasiRNA (tasiR255) and TST-AGO1 in t1 transgenic lines. The graph at the top shows the mean (t1) relative to tasiR255 levels +the SD (Col-0=1.0). One blot from three biological replicates is shown. Each biological replicate is a pool of at least eight independent lines that were randomly selected. U6 and L-Rubisco blots are shown as loading controls. Other details are as in (C).

(Fig. 1A). As a control, the pAGO1:TST-GFP construct, designed to express TST-tagged GFP under the same AGO1 regulatory sequences, was also generated (Fig. 1A). To test the functionality of TST-AGO1, pAGO1:TST-AGO1 and pAGO1:TST-GFP constructs were transformed in both Col-0 and ago 1-25 genetic backgrounds. At least 24 independent T<sub>1</sub> transgenic lines were recovered for each construct in both backgrounds. Interestingly, ago 1-25 phenotypic defects, such as slow growth or delayed flowering, were suppressed in plants expressing pAGO1:TST-AGO1, but not in plants expressing pAGO1:TST-GFP (Fig. 1B, C). In contrast, plants expressing either construct in the Col-0 background were phenotypically similar to non-transformed Col-0 plants (Fig. 1B, C). Importantly, plants expressing pAGO1: TST-AGO1 or pAGO1-TST-GFP constructs accumulated high levels of TST-AGO1 and TST-GFP proteins, respectively, as observed in the western blot analysis (Fig. 1D). To further investigate TST-AGO1 functionality, AGO1-dependent TAS1c trans-acting siRNA (tasiRNA) 255 (tasiR255) formation was analyzed in T<sub>1</sub> transgenic plants. TasiR255 accumulation levels were restored to Col-0 levels in ago1-25 plants transformed with pAGO1:TST-AGO1 but not in ago1-25 plants transformed with pAGO1:TST-GFP (Fig. 1D). Finally, tasiR255 levels in transgenic lines expressing either construct in the Col-0 background were similar to those of non-transformed Col-0 plants. Overall, these results indicate that the addition of a TST tag at the 5' terminus of Arabidopsis AGO1 does not affect AGO1 functionality. They also suggest that the expression of TST-AGO1 in a Col-0 background does not impair plant growth or AGO1 functionality.

AP-MS analysis of AGO1 protein complexes in response to Cu-deficiency stress

Given the previously described key role of miRNA-mediated gene regulation in response to Cu deficiency (Pilon, 2017;

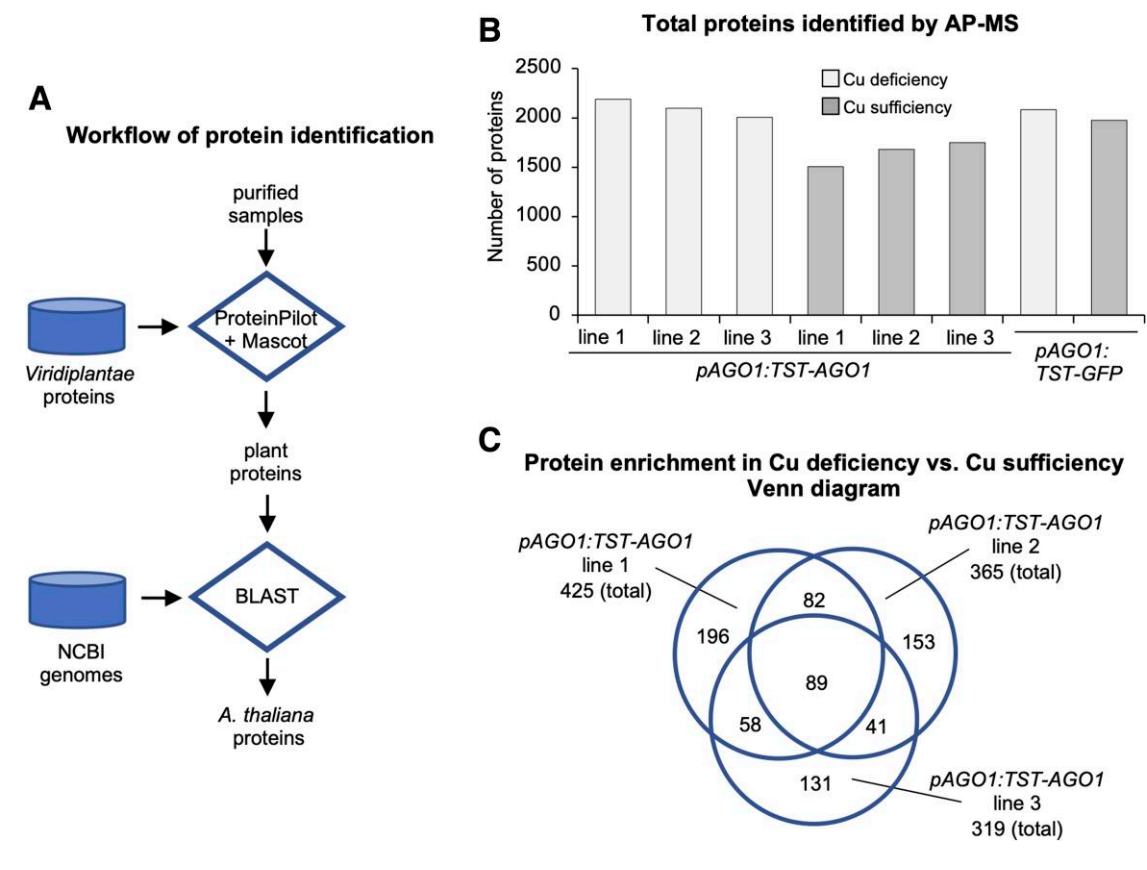
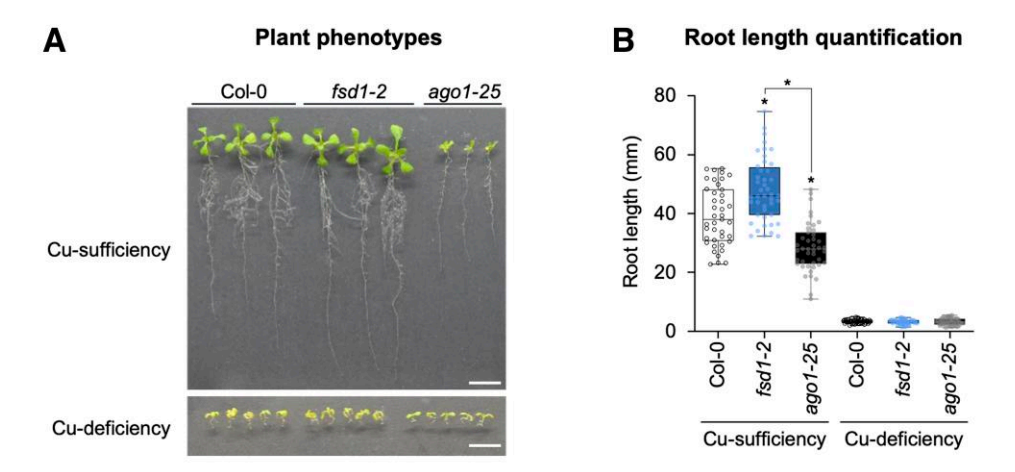


Fig. 2. Protein analyses in TST-AGO1 complexes purified by AP-MS. (A) Flowchart of the process for plant protein identification. Proteins from purified samples are processed through ProteinPilot and Mascot software tools, and identified proteins are matched against the Viridiplantae protein database to filter for plant proteins. The plant proteins are further analyzed using the Blast tool against the NCBI Genomes database to identify Arabidopsis-specific proteins. (B) Bar chart showing the total number of proteins identified by AP-MS in the three different pAGO1-TST-AGO1 transgenic lines grown under copper (Cu) deficiency (light gray bars) or Cu sufficiency (dark gray bars). (C) Venn diagram comparing the total number of proteins in Cu deficiency versus Cu sufficiency identified in the three pAGO1:TST-AGO1 transgenic lines. The cut-off value for significant fold change is set at log<sub>2</sub> fold=1, meaning that only proteins enriched in Cu deficiency versus Cu sufficiency are represented. The overlapping section indicates the proteins identified in purified samples from independent transgenic lines.

Perea-García et al., 2022), we analyzed the AGO1 protein interactome under Cu deficiency compared with Cu sufficiency, using three independent T<sub>4</sub> pAGO1:TST-AGO1 transgenic lines to study AGO1 function in both conditions: lines 1, 2, and 3. As a negative control, one T<sub>4</sub> pAGO1:TST-GFP transgenic line was also grown in parallel under the same conditions. Seedlings of each transgenic line were grown for 10 d under Cu-sufficiency (1 µM CuSO<sub>4</sub>) or Cu-deficiency (100 µM BCS) conditions. AGO1 and GFP protein complexes were purified by affinity chromatography in native conditions. Proteins from the purified complexes were resolved using denaturing PAGE and subsequently subjected to in-gel digestion with trypsin. The resulting peptides were extracted from the gel and analyzed by LC coupled with tandem MS to identify the proteins in the purified complexes. All hits resulting from proteomic analysis of complexes purified from seedlings of each transgenic line grown under Cu sufficiency and Cu deficiency are shown in Supplementary Dataset S2.

Next, we examined the dynamics of the AGO1 protein interactome in response to Cu deficiency. Proteins from purified samples were processed using the ProteinPilot (Shilov et al., 2007) and Mascot (Perkins et al., 1999) software tools, and the identified proteins were matched against the Viridiplantae protein database to filter for plant-specific proteins (Fig. 2A). These plant proteins were further analyzed using the BLAST tool (Altschul et al., 1990) against the NCBI Genomes to identify Arabidopsis-specific proteins. The total numbers of proteins identified in the three pAGO1:TST-AGO1 lines under Cu deficiency were similar (2185, 2099, and 2002 for lines 1, 2 and 3, respectively), although higher than the number observed in all lines under Cu sufficiency (1565, 1680, and 1749 for lines 1, 2, and 3, respectively) (Fig. 2B). The total number of proteins identified in the pAGO1:TST-GFP line under Cu deficiency and sufficiency was rather similar (2080 and 1975, respectively) (Fig. 2B). We then quantified the change in the abundance of AP-MS interactors under these



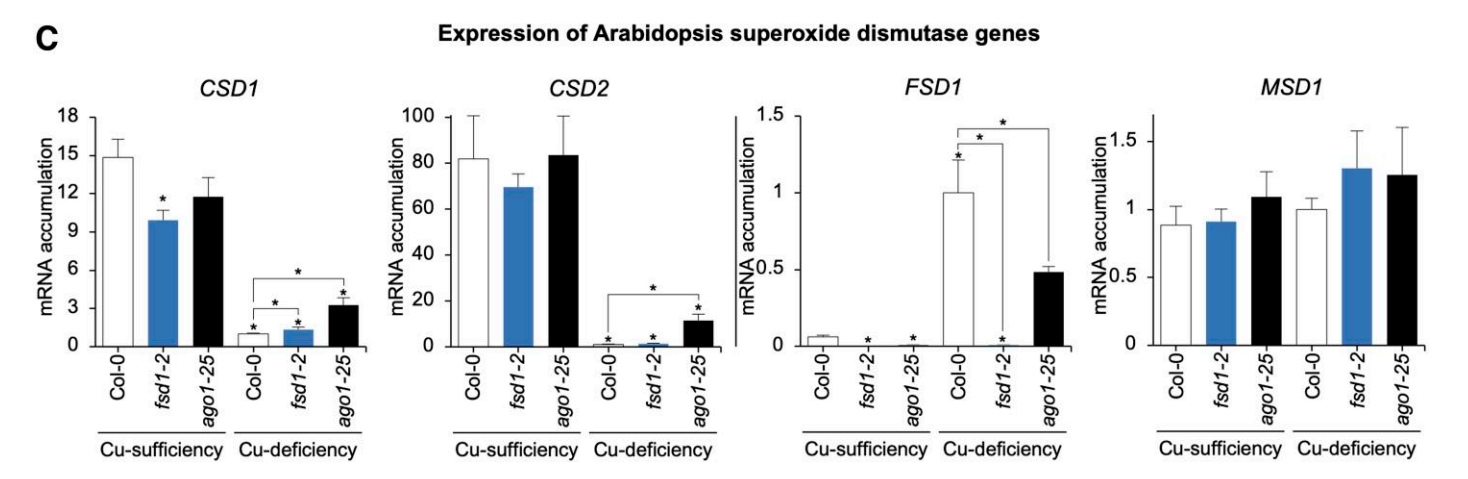
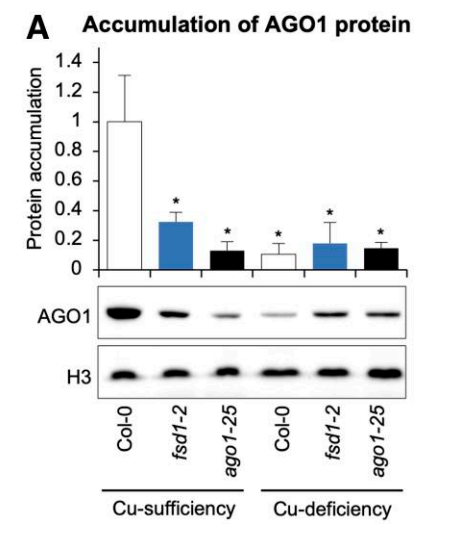


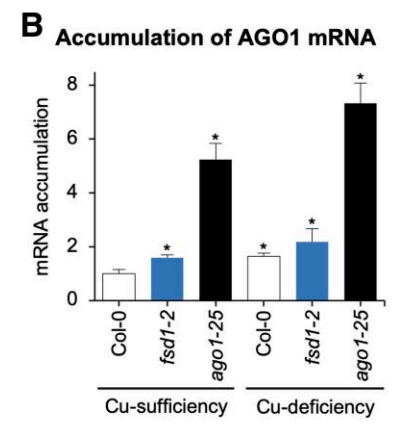
Fig. 3. Analysis of Arabidopsis superoxide dismutase genes under Cu-sufficiency and -deficiency conditions in Col-0, *fsd1-2*, and *ago1-25* seedlings. (A) Photographs of 10-day-old Col-0, *fsd1-2*, and *ago1-25* seedlings grown on plates with MS medium in Cu sufficiency (1 μM Cu) or deficiency (100 μM BCS). (B) Quantification of root length of Col-0, *fsd1-2*, and *ago1-25* seedlings grown in the same conditions as in (A). Mean relative level (*n*=40–45) +the SD of root length. Pairwise Student's *t*-test comparisons are represented with an \* if significantly different (*P*<0.05) compared with Col-0 in each condition. (C) Relative expression of *CSD1*, *CSD2*, *FSD1*, and *MSD1* mRNAs determined by RT–qPCR in 10-day-old Col-0, *fsd1-2*, and *ago1-25* seedlings, grown under control (Cu sufficiency, 1 μM CuSO<sub>4</sub>) and Cu deficiency (100 μM BCS). Mean relative level (*n*=3) +the SE of mRNAs after normalization to *ACTIN2*. Bars with an \* indicate significant differences from the Col-0 control sample (*P*<0.05 in all pairwise Student's *t*-test comparisons). Other *t*-test comparisons are also shown. Each biological replicate is a pool of at least 20 independent lines that were randomly selected.

two conditions (Supplementary Dataset S3), discarding those proteins present in the *pAGO1:TST-GFP* control purifications. A log<sub>2</sub> fold change value was assigned for each protein comparison, with log<sub>2</sub> fold >0 indicating that the protein is more abundant in Cu deficiency and log<sub>2</sub> fold <0 indicating higher abundance in Cu sufficiency. A Venn diagram showed that 89 proteins were more abundant in Cu deficiency than in Cu sufficiency in the three lines (Fig. 2C; Supplementary Dataset S4). Among these proteins, we considered FeSOD1 for our subsequent analyses, as it was recently identified as an AGO1 interactor in yeast two-hybrid assays (Bressendorff *et al.*, 2023) and was also known to participate in oxidative stress responses in a Cu-dependent manner (Melicher *et al.*, 2022).

AGO1 and FeSOD1 fine-tune Cu-responsive SOD gene expression

To assess the impact of Cu deficiency on plant growth, Arabidopsis Col-0, *fsd1-2* (loss-of-function mutant for *FSD1*), and *ago1-25* (mutant for *AGO1*) seedlings were grown under Cu-sufficient and Cu-deficient conditions (Fig. 3A), and their root lengths were quantified (Fig. 3B). Under Cu sufficiency, all genotypes displayed healthy growth, with *fsd1-2* seedlings showing a slight but statistically significant increase in root length compared with Col-0 (*P*<0.05), while *ago1-25* seedlings exhibited a pronounced decrease as observed before in other *ago1* mutants (Trolet *et al.*, 2019). Under Cu deficiency, root growth was significantly inhibited across all genotypes (Fig. 3A, B).





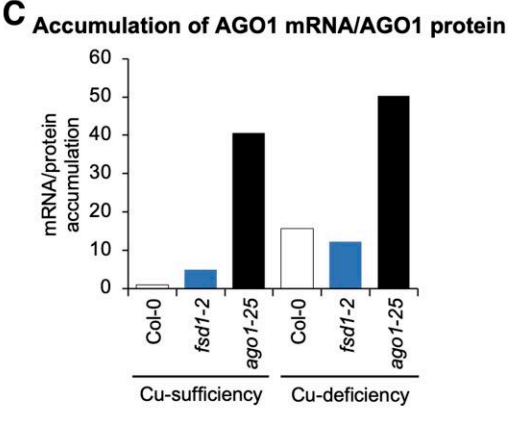


Fig. 4. Accumulation of AGO1 protein and mRNA in Arabidopsis Col-0, fsd1-2, and ago1-25 seedlings. (A) Accumulation of endogenous AGO1 protein in 10-day-old Col-0, fsd1-2, and ago1-25 seedlings, grown under control (Cu sufficiency) and Cu deficiency. The graph at the top shows the mean (n=3) relative to endogenous AGO1 levels +the SD (Col-0=1.0). One blot from three biological replicates is shown. Each biological replicate is a pool of at least 20 independent lines that were randomly selected. The HISTONE H3 (H3) blot is shown as loading control in total protein extracts. (B) Relative expression of AGO1 determined by RT-qPCR in 10-day-old Col-0, fsd1-2, and ago1-25 seedlings, grown under control and Cu deficiency. Mean relative level (n=3) +the SE of mRNA after normalization to ACTIN2 (Col-0=1.0). Bars with an \* indicate significant differences from the Col-0 control sample (P<0.05 in all pairwise Student's t-test comparisons). Each biological replicate is a pool of at least 20 independent lines that were randomly selected.

Expression of SOD genes is an excellent marker for Cu status in plant cells (Yamasaki et al., 2009; Andrés-Colás et al., 2013). To examine SOD expression under our experimental conditions, mRNA accumulation of CSD1, CSD2, FSD1, and MSD1 was measured by RT-qPCR (Fig. 3C) in Col-0, fsd1-2, and ago1-25 seedlings. As previously reported (Yamasaki et al., 2009), expression of Cu/Zn SODs encoded by CSD1 and CSD2 in Col-0 seedlings was high under Cu sufficiency but remained low under Cu deficiency (Fig. 3C). Although the expression pattern in ago1-25 was similar, CSD expression was significantly higher in most cases (Fig. 3C). Since CSD expression is regulated by miR398, the impaired AGO1 function in ago1-25 could explain this difference. On the other hand, expression of FeSOD1, encoded by FSD1, remained low under Cu sufficiency and was higher under Cu deficiency in both genotypes, although it was significantly lower in ago 1-25 under Cu deficiency (Fig. 3C). This suggests an indirect effect of AGO1 function on FSD1 transcription under Cu deficiency, potentially due to miR156 influencing the ratio of different SPL members and thereby affecting the occupancy by SPL7 of Cu-deficiency target promoters (Perea-García et al., 2021). Finally, expression of MnSOD, encoded by MSD1, remained approximately constant across both genotypes and conditions (Fig. 3C).

FeSOD1 is essential for AGO1 stability, particularly under Cu deficiency

Next, we first investigated whether FeSOD1 function was required for proper AGO1 expression. To do so, AGO1 protein levels were measured by western blot in 10-day-old Col-0, fsd1-2, and ago1-25 seedlings grown under Cu-sufficiency and Cu-deficiency conditions (Fig. 4A). Surprisingly, AGO1 protein levels in Col-0 plants drastically dropped (~90%) in Cu deficiency compared with Cu sufficiency. This decrease was similar to that observed in ago 1-25 plants grown under both Cu conditions. Additionally, AGO1 protein levels also decreased by ~80% in fsd1-2 seedlings compared with Col-0 plants under Cu sufficiency (Fig. 4A). These results indicate an important decrease in AGO1 protein in Col-0 plants grown under Cu deficiency, and in fsd1-2 seedlings grown under both Cu conditions.

To further investigate whether the reduction in AGO1 protein levels was due to transcriptional regulation, we analyzed AGO1 mRNA levels by RT-qPCR (Fig. 4B) in the same samples used for AGO1 protein analysis (Fig. 4A). Under Cu sufficiency, AGO1 transcript levels were significantly higher in fsd1-2 compared with Col-0, suggesting that FeSOD1 function may influence AGO1 expression. Additionally, ago1-25 mutants exhibited a significant increase in AGO1 mRNA levels relative to Col-0, probably due to impaired miR168-mediated AGO1 mRNA regulation caused by reduced AGO1 activity (Vaucheret et al., 2006). Under Cu deficiency, AGO1 transcript accumulation markedly increased in Col-0, fsd1-2, and ago1-25 seedlings compared with Cu sufficiency, with ago 1-25 displaying the highest expression levels (Fig. 4B). These results indicate that the reduction in AGO1 protein levels under Cu deficiency is not due to decreased AGO1 transcript accumulation. Finally, northern blot analysis showed that under Cu sufficiency miR 168 levels decline modestly ( $\sim$ 15%) in fsd1-2 but greatly in ago1-25 ( $\sim$ 60%) compared

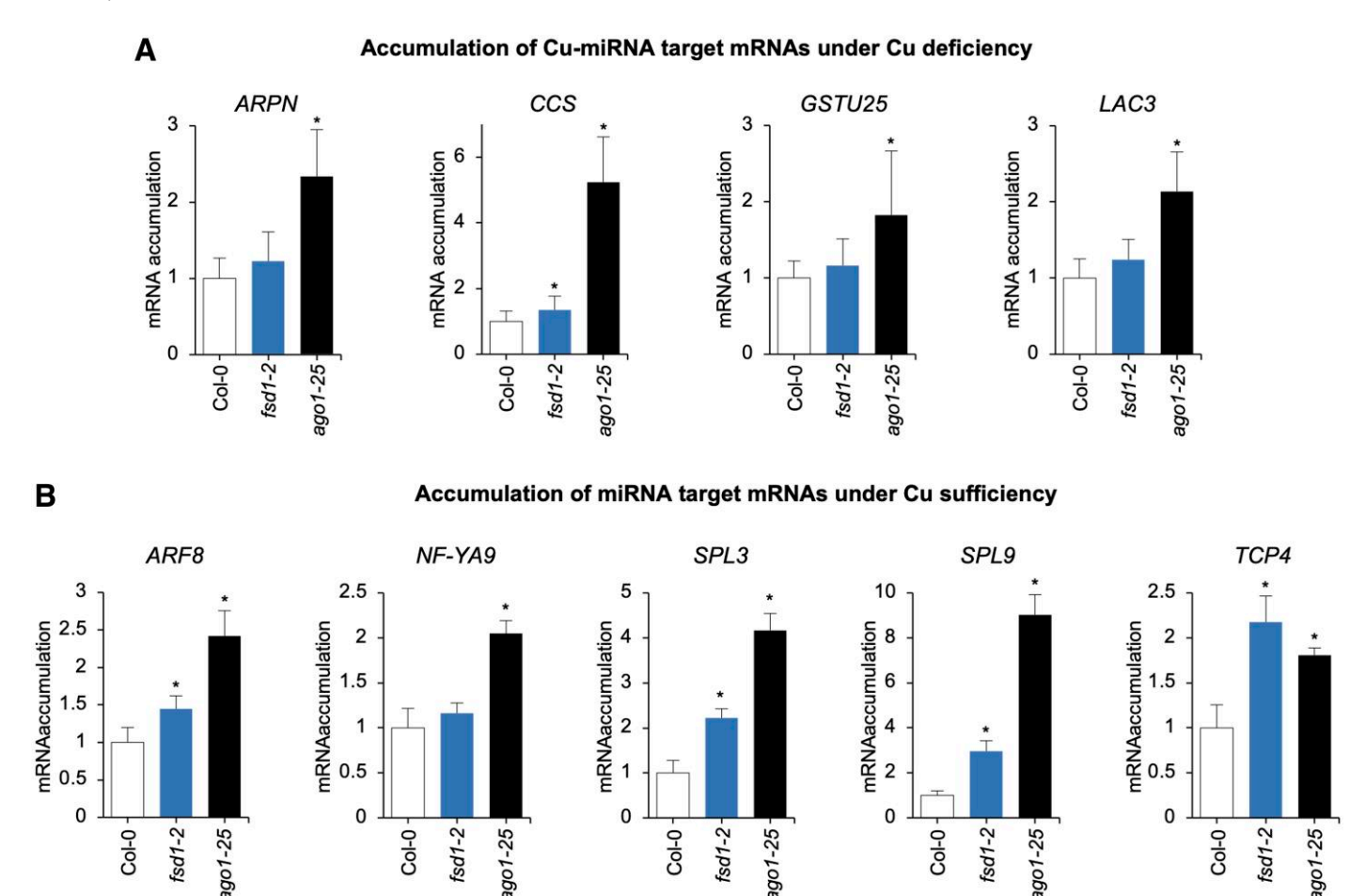


Fig. 5. Accumulation of miRNA target genes in Arabidopsis Col-0, fsd1-2, and ago1-25 seedlings. (A) Relative expression of Cu-miRNA targets ARPN, CCS, LAC3, and GSTU25 determined by RT-qPCR in 10-day-old Col-0, fsd1-2, and ago1-25 seedlings, grown under Cu deficiency. Mean relative level (n=3) +the SE of mRNAs after normalization to ACTIN2 (Col-0=1.0). Bars with an \* indicate significant differences from the Col-0 control sample (P<0.05 in all pairwise Student's t-test comparisons). Each biological replicate is a pool of at least 20 independent lines that were randomly selected. (B) Relative expression of miRNA targets ARF8, NF-YA9, SPL3, SPL9, and TCP4 determined by RT-qPCR in 10-day-old Col-0, fsd1-2, and ago1-25 seedlings, grown under Cu sufficiency (1 μM CuSO<sub>4</sub>). Other details are as in (A).

with Col-0 (Supplementary Fig. S1). Under Cu deficiency, miR168 remains essentially unchanged in Col-0, falls slightly in *fsd1-2*, but decreases considerably to ~35% in *ago1-25*. This gradient inversely mirrors the AGO1 mRNA profile (Fig. 4B), supporting the expected negative feedback between miR168 abundance and AGO1 transcript levels described before (Vaucheret *et al.*, 2006).

To further assess the relationship between AGO1 mRNA and protein levels, we calculated the relative ratio of AGO1 mRNA to AGO1 protein accumulation in the same samples (Fig. 4C). Under Cu sufficiency, this ratio (R) was much higher in fsd1-2 (R=4.9) and ago1-25 (R=40.6) mutants compared with Col-0 (R=1), indicating that despite increased AGO1 transcript levels, AGO1 protein accumulation remained low in these mutants. Under Cu deficiency, the AGO1 mRNA/ protein ratio increased more drastically across all genotypes, particularly in ago1-25, which exhibited the highest ratio (R=50.2) among the conditions tested.

To check whether Cu deficiency induces oxidative stress,  $H_2O_2$  levels were measured by using a KI-based colorimetric assay (Junglee *et al.*, 2014) in 10-day-old Arabidopsis Col-0 seedlings grown under Cu-sufficiency and -deficiency conditions (Supplementary Fig. S2). Results show a significant increase in  $H_2O_2$  content (from ~15 nmol g<sup>-1</sup> FW in seedlings grown under Cu sufficiency to ~75 nmol g<sup>-1</sup> FW in seedlings grown under Cu deficiency), indicating that ROS are increased upon Cu-deficiency conditions.

Finally, to test whether oxidative stress *per se* destabilizes AGO1, the accumulation of AGO1 protein was also analyzed in Col-0, *fsd1-2*, and *ago1-25* seedlings under oxidative (MV) or heavy metal (Cd) stresses (Supplementary Fig. S3). While the treatment with MV is de-stabilizing AGO1 by reducing AGO1 protein accumulation to ~0.5 in wild-type Col-0 plants, indicating that superoxide-driven oxidative stress promotes AGO1 degradation, Cd treatment led to an increase in AGO1 abundance in all three genotypes, suggesting that

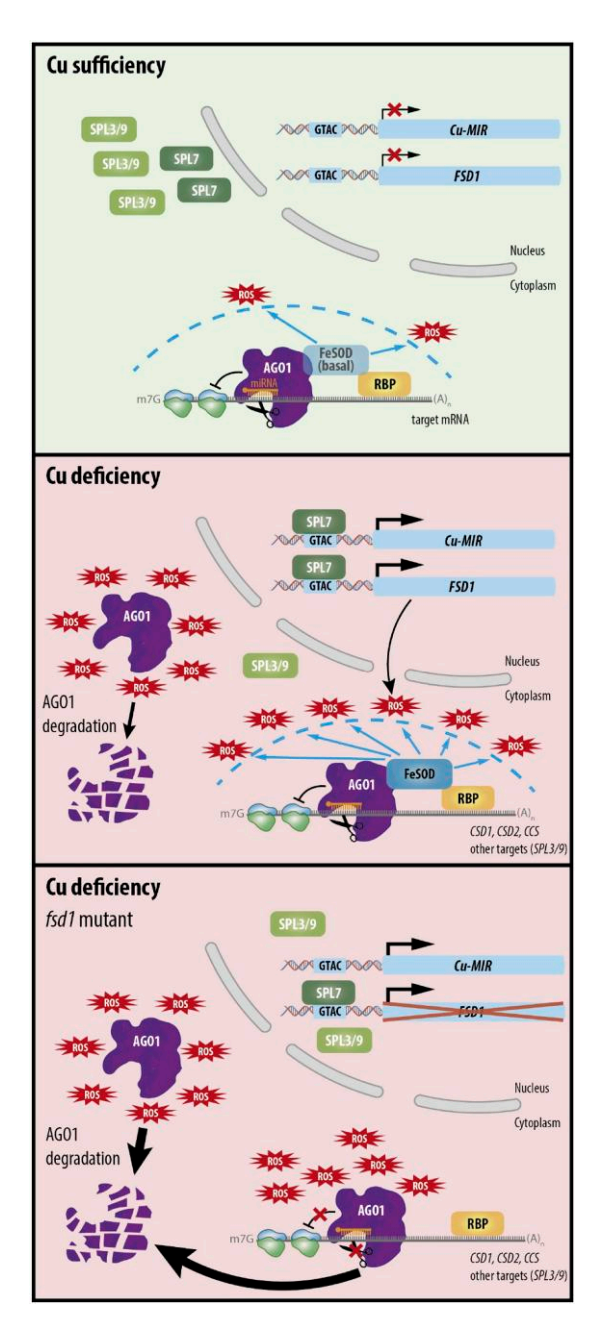


Fig. 6. Model for the anti-superoxide protection of the AGO1 function by the FeSOD1 dome under Cu deficiency. Top, under Cu sufficiency Cu-miRNA and FSD1 expression are essentially blocked. A basal level of iron superoxide dismutase FeSOD1 allows the protection of AGO1 from reactive oxygen species (ROS) derived from normal cellular metabolism. Middle, under Cu deficiency, the increase presence of ROS, including superoxide anion, induces a certain level of AGO1 degradation. However, in these conditions, SPL7 outcompetes SPL3 and SPL9 for binding to cis-regulatory transcriptional elements (GTACs) present in promoters of Cu-miRNA genes and FeSOD1-encoding FSD1, inducing their expression. Increased levels of FeSOD1 play a protective role for the effector complex of RNAi by detoxifying superoxide anions. By directly interacting with AGO1 and/or associated RNA-binding proteins (RBPs), FeSOD1 promotes AGO1 stability, contributing to Cu-miRNA and general AGO1 functions. Bottom: in fsd1 mutants. the lack of FeSOD impedes proper detoxification of ROS and leads to AGO1 degradation in both Cu-sufficiency (left) and Cu-deficiency (right) conditions.

AGO1 stability under Cd stress is maintained irrespective of the presence of FeSOD1.

Copper availability modulates the protective role of FeSOD1 in maintaining AGO1 function

To determine whether the decrease in AGO1 protein content also affected its functionality under Cu deficiency, the expression of several Cu-miRNA targets (ARPN, miR160 target; CCS, CSD1, and CSD2, miR398 targets; GSTU25, miR396 target; LAC3, miR397 target) was analyzed by RT-qPCR in 10-day-old Col-0, fsd1-2, and ago 1-25 seedlings (Fig. 5A). As expected, the expression of all Cu-miRNA targets (except for GSTU25) significantly increased in ago1-25 compared with Col-0. Similarly, all miRNA targets were induced to varying degrees in fsd1-2 compared with Col-0, with the increase in CSD1 being statistically significant (Fig. 5A). These findings confirm that AGO1 functionality requires the presence of FeSOD1 under Cu deficiency.

Next, we wondered whether FeSOD1 activity was also required for general AGO1 function under Cu sufficiency and for regulating other non-Cu-miRNA targets. The expression of different well-known miRNA targets (ARF8, miR167 target; NF-YA9, miR169 target; SPL3 and SPL9, miR156 targets; TCP4, miR319 target) was analyzed by RT-qPCR in 10-day-old Col-0, fsd1-2, and ago1-25 seedlings grown under Cu sufficiency (Fig. 5B). As expected, the expression of all miRNA targets was significantly higher in ago 1-25 compared with Col-0. Interestingly, the expression of all miRNA targets also increased in fsd1-2 compared with Col-0, with a statistically significant increase observed for four out of five miRNA targets (ARF8, SPL3, SPL9, and TCP4). Notably, the increased expression of miR156 targets (SPL3 and SPL9) is relevant, as these targets compete with SPL7 in Cu-deficiency responses (Perea-García et al., 2021). Finally, the expression of the miRNA targets mentioned above was also analyzed in seedlings of the different genotypes grown under Cu deficiency (Supplementary Fig. S4). The expression of all miRNA targets was higher in both fsd1-2 and ago1-25 compared with Col-0, although this increase was significant only for NF-YA9 and SPL3 in ago 1-25 (Supplementary Fig. S4).

In conclusion, our results indicate that FeSOD1 is necessary for proper AGO1 function in miRNA-mediated gene silencing. We propose a model (Fig. 6) in which the superoxide dismutase activity of FeSOD1 protects against oxidative stress, contributing to the increased stability of the AGO1 protein. This protective role of FeSOD1 is especially important under Cu deficiency due to the elevated oxidative stress and the critical role played by Cu-miRNAs in the response of the plant to this nutrient deficit. Absence of FeSOD1 in fsd1-2 mutants results in AGO1 degradation independently of the Cu levels (Fig. 6).

## **Discussion**

This study investigates plant responses under Cu-deficiency conditions, where Cu-miRNAs regulate the mRNAs encoding cuproproteins. Different studies have reported that numerous miRNAs are induced by a variety of environmental stresses, suggesting the existence of shared signaling pathways (Martin et al., 2010). Plants face a conflicting situation when responding to adverse conditions, give the extensive role of miRNAs in stress responses and the instability of the key protein AGO1 within the RISC under suboptimal conditions (Fang and Qi, 2016). To resolve this conflict, providing a protective environment to preserve AGO1 function could be crucial for an effective stress response. Here, we explored how Cu deficiency influences the regulation of miRNA targets mediated by AGO1. We analyzed the AGO1 protein interactome in pAGO1:TST-AGO1 Arabidopsis transgenic plants grown under both normal and Cu-deficient conditions. Due to the adverse effects of Cu deficiency on AGO1 function, we searched for interactor proteins with a protective effect on AGO1. Notably, a well-documented response to Cu deficiency is the substitution of Cu/ZnSODs with FeSODs to support antioxidative defense (Yamasaki et al., 2009). In this context, FeSOD1 was enriched in TST-AGO1 complexes purified from all three pAGO1:TST-AGO1 lines grown in Cu deficiency. Since FeSOD1 was recently identified as an AGO1 interactor in yeast two-hybrid assays (Bressendorff et al., 2023), the role of FeSOD1-AGO1 interaction became the main focus of our study.

Particularly striking is the opposite pattern observed between AGO1 mRNA and protein levels, suggesting that either AGO1 translation or stability is severely compromised under Cu deficiency. This is evidenced by the significant decrease in endogenous AGO1 protein levels in Col-0 plants grown under Cu-deficient conditions compared with Cu-sufficient conditions. A similar opposite pattern is also observed in fsd1-2 and, more drastically, in the ago1-25 mutant, possibly indicating a compensatory increase in AGO1 mRNA synthesis in response to low AGO1 protein levels (Fig. 4).

The elevated ROS levels induced by Cu deficiency (Supplementary Fig. S2) appear to be a key factor explaining AGO1 degradation, as the presence of FeSOD1 detoxifies the cellular oxidative state and safeguards AGO1 function in regulating Cu-miRNA genes or other known targets (Figs 5A, 6; Supplementary Fig. S4). Consistently, as peroxide is the reaction product of SODs, the peroxidase PRX32 is also identified as an antioxidant molecule interacting with AGO1 under Cu deficiency (Supplementary Dataset S4). Whether ROS-induced AGO1 degradation occurs via the ubiquitinproteasome system, the autophagy pathway, or simultaneously through both remains unknown. It is possible that specific proteins target AGO1 for degradation, as reported for the F-box protein FBW2 that assembles an SCF complex that selectively targets AGO1 for proteolysis when it is unloaded (Hacquard et al., 2022).

Alongside Cu-miRNAs, SPL7 can also induce FSD1 expression (Yamasaki et al., 2009). Our results indicate that defects in AGO1 function impact Cu-miRNAs and FSD1 expression (Fig. 3C). The reduced expression of FSD1 in ago 1-25 probably results from defective miR 156 targeting. Indirectly, FSD1 expression is affected by miR156, whose main function is to inhibit the gene expression of some members of the SPL protein family (especially SPL3), while it does not affect other members such as SPL7. The purpose seems to be reducing competition between SPL factors for target promoter binding (Perea-García et al., 2021). Consequently, the defective targeting of miR156 in ago1-25 explains the increased expression of non-SPL7 members (SPL3 and SPL9), potentially disrupting SPL7 responses, including FSD1 expression (Fig. 5). Additionally, the expression of miR398 targets, CSD genes and CCS, is also reduced in ago 1-25 (Fig. 3C).

An unresolved question concerns the intracellular site of FeSOD1-mediated protection of AGO1. AGO1 is mainly cytosolic, concentrated on the cytosolic face of the rough endoplasmic reticulum, and enters the nucleus only transiently during miRNA loading (Brodersen et al., 2012; Bologna et al., 2018). FSD1, although mainly plastidic, also has verified cytoplasmic and nuclear pools (Dvořák et al., 2021). Consequently, the FeSOD1-mediated protection of AGO1 most plausibly occurs in the cytoplasm, but a nuclear contribution cannot be excluded. In any case, to test whether the FeSOD1-AGO1 interaction functions reciprocally, we examined the role of FeSOD1 in AGO1 function. FeSOD1 is essential for ROS response, specifically in eliminating superoxide radicals (Ravet and Pilon, 2013). In this sense, the interaction between AGO1 and FeSOD1 suggests that antioxidant protection is necessary for AGO1 function. To check this, we studied the AGO1 protein content in fsd1-2 mutants. Homozygous fsd1-2 seedlings grown under Cu-deficient and Cu-excess conditions exhibit reduced ROS neutralization, affecting phenotypes such as increased chlorosis (Melicher et al., 2022). Moreover, this capacity depends on Cu availability, as FSD1 expression is regulated by Cu status. AGO1 levels depend on Cu status and the presence of FeSOD1, supporting the hypothesis that Cu deficiency and FeSOD1 have a protective role against oxidative damage to AGO1 (Fig. 3B). Furthermore, the effects on different Cu-miRNA targets (ARPN, CCS, CSD2, GSTU25, and LAC3) (Fig. 5A) highlight the defect in AGO1 function in the absence of this protective barrier. Taken together, our findings reveal the challenges plants face under Cu deficiency in maintaining RNAi efficiency, given the essential role of Cu-miRNAs and the stability of AGO1 protein under these conditions. The substitution of Cu/ZnSOD with FeSOD1 serves as a solution to this compromise (Fig. 6). Increased Fe demand for FeSOD1 highlights the interaction

between Cu and Fe homeostasis (Waters et al., 2012; Perea-García et al., 2021). Notably, IRT1, the main Fe transporter, was enriched in TST-AGO1 complexes purified under Cu deficiency. Further studies are needed to clarify the role of the AGO1-IRT1 interaction, although an indirect association via IRT1-RNA-binding proteins with the RISC may be plausible.

While stress conditions often reveal molecular imbalances, such as RNAi functioning with unstable AGO1, these balances could also exist under normal conditions, as observed here for AGO1 under Cu sufficiency. Despite low FSD1 levels under Cu sufficiency, the expression of non-Cu-miRNAs, such as miR167 (ARF8) (Wu et al., 2006), miR169 (NF-YA9) (Sorin et al., 2014), miR156 (SPL3 and SPL9) (Kim et al., 2012), and miR319 (TCP4) (Palatnik et al., 2007), was also affected in fsd1-2 (Fig. 5B). These findings suggest a broader scenario (Fig. 6) where maintaining an antioxidant environment around AGO1 is crucial for proper RNAi function, particularly under Cu deficiency.

Finally, whether FeSOD1-mediated protection of AGO1 extends to other stressors remains unexplored. Our preliminary analyses in Col-0, fsd1-2, and ago1-25 seedlings exposed to oxidative stress (MV) or heavy metal (Cd) stress revealed distinct effects of these treatments on AGO1 abundance. MV treatment decreased AGO1 accumulation in all three genotypes (Supplementary Fig. S3), an effect qualitatively similar though less pronounced than that caused by Cu deficiency. In contrast, Cd exposure increased AGO1 protein levels to comparable values in all genotypes, indicating that AGO1 stability under Cd stress does not rely on FeSOD1. Cd stress is known to elevated ROS, mainly as H<sub>2</sub>O<sub>2</sub> (Liu et al., 2010), and to trigger a broad transcriptional reprogramming that down-regulates most miRNAs (Pegler et al., 2021). It is possible that reduced miR168 abundance, together with a ROS environment richer in H<sub>2</sub>O<sub>2</sub> than superoxide, allows higher AGO1 transcript and protein accumulation, thereby offsetting Cd-induced oxidative stress. Conversely, MV triggers superoxide directly (Scarpeci et al., 2008), reinforcing the idea that (i) the quality of ROS may determine whether AGO1 is protected or degraded, and (ii) FeSOD1 protection is most critical when superoxide predominates, as under Cu deficiency, whereas Cd-induced H<sub>2</sub>O<sub>2</sub> permits AGO1 accumulation independently of FeSOD1. In any case, our findings raise two open questions: (i) does repressing AGO1 activity under oxidative stress confer any adaptive advantage, for example by transiently limiting miRNA-guided down-regulation of stress-responsive transcripts? and (ii) is the FeSOD1-AGO1 interaction itself conditionally modulated to counteract oxidative damage, thereby preserving AGO1 protein levels and activity only when superoxide-driven stress is severe? Clarifying miR168 dynamics, ROS partitioning, and possible regulation of the FeSOD1-AGO1 nexus will illuminate how plants fine-tune RNA interference to maintain redox and metal homeostasis.

## Supplementary data

The following supplementary data are available at *JXB* online.

Dataset S1. Nucleotide and amino acid sequences of TST-based inserts. Dataset S2. Proteins identified by AP-MS in pAGO1:TST-AGO1 and pAGO1:TST-GFP transgenic lines grown under Cu deficiency and Cu

Dataset S3. Proteins identified by AP-MS in each of the three pAGO1: TST-AGO1 transgenic lines grown under Cu deficiency versus Cu sufficiency, and not present in pAGO1:TST-GFP AP-MS samples for each condition.

Dataset S4. Proteins identified by AP-MS in all three pAGO1: TST-AGO1 transgenic lines grown under Cu deficiency versus Cu sufficiency, and not present in pAGO1:TST-GFP AP-MS samples for each condition.

Fig. S1. Accumulation of miR168 in Arabidopsis Col-0, fsd1-2, and ago 1-25 seedlings.

Fig. S2. Quantification of hydrogen peroxide (H<sub>2</sub>O<sub>2</sub>) content in Arabidopsis Col-0 seedlings under Cu sufficiency and deficiency.

Fig. S3. AGO1 protein accumulation in Arabidopsis Col-0, fsd1-2, and ago 1-25 seedlings under oxidative and heavy metal stress.

Fig. S4. Accumulation of miRNA target mRNAs in different Arabidopsis genotypes under Cu deficiency.

Table S1. Name, sequence, and use of oligonucleotides employed in the present study.

## **Ackowledgements**

We thank Sara Toledano-Franco for excellent technical assistance, Dr Tomás Takác for sharing fsd1-2 seeds, and Carlos Fuentes from the Proteomics Unit of University of Córdoba for assistance in preparing and analyzing purified proteins.

## **Author contributions**

AC and LP: planned and designed the research and wrote the manuscript with input from the rest of the authors; AHT, APG, AC, AEC, LLD, AAB, and MO: performed most of the experiments; JSV and JAD: performed AGO1 affinity purifications; GR: carried out the computational analysis of AP-MS samples; AHT, APG, LP, and AC: analyzed data.

## Conflict of interest

The authors declare no conflict of interest.

## **Funding**

This work was supported by grants or fellowships from MCIN/AEI/ 10.13039/501100011033 (co-financed by the European Regional Development Fund) [RTI2018-095118-A-I00, PID2021-122186OB-I00 and RYC-2017-21648 to AC; PID2021-127671NB-I00 to GR; PID2020-116940RB-I00 to LP and APG; BIO2017-83184-R and PID2020-114691RB-I00 to JAD; PRE2019-088439 to AEC], and from the Generalitat Valenciana (CIPROM/2022/21 to GR and JAD).

#### Data availability

All data relating to this manuscript can be found within the manuscript and its supplementary files. Data that support the findings of this study are available from the corresponding authors upon reasonable request. The mass spectrometry proteomics data have been deposited in the

ProteomeXchange Consortium via the PRIDE (Perez-Riverol et al., 2022) partner repository with the dataset identifier PXD057108.

#### References

Abramoff M, Magalhaes P, Ram S. 2004. Image processing with ImageJ. Biophotonics International 11, 36-42.

Altschul SF, Gish W, Miller W, Myers EW, Lipman DJ. 1990. Basic local alianment search tool. Journal of Molecular Biology 215, 403-410.

Gómez-Muñoz N, Giménez-Santamarina Sánchez-Vicente J. Navarro-López J. Martínez F. Daròs J-A. Rodrigo G. 2021. Molecular signatures of silencing suppression degeneracy from a complex RNA virus. PLoS Computational Biology 17, e1009166.

Andrés-Colás N, Perea-García A, Mayo de Andrés S, Garcia-Molina A, Dorcey E, Rodríguez-Navarro S, Pérez-Amador MA, Puig S, Peñarrubia L. 2013. Comparison of global responses to mild deficiency and excess copper levels in Arabidopsis seedlings. Metallomics 5, 1234-1246.

Baumberger N, Baulcombe DC. 2005. Arabidopsis ARGONAUTE1 is an RNA slicer that selectively recruits microRNAs and short interfering RNAs. Proceedings of the National Academy of Sciences, USA 102, 11928–11933.

Bernal M, Casero D, Singh V, et al. 2012. Transcriptome sequencing identifies SPL7-regulated copper acquisition genes FRO4/FRO5 and the copper dependence of iron homeostasis in Arabidopsis. The Plant Cell 24, 738-761.

Bologna NG, Iselin R, Abriata LA, Sarazin A, Pumplin N, Jay F, Grentzinger T, Dal Peraro M, Voinnet O. 2018. Nucleo-cytosolic shuttling of ARGONAUTE1 prompts a revised model of the plant microRNA pathway. Molecular Cell 69, 709-719.e5.

Borges F, Martienssen RA. 2015. The expanding world of small RNAs in plants. Nature Reviews. Molecular Cell Biology 16, 727-741.

Bressendorff S, Kausika S, Zobbe Sjøgaard IMZ, Oksbjerg ED, Michels A, Poulsen C, Brodersen P. 2023. The N-coil and the globular N-terminal domain of plant ARGONAUTE1 are interaction hubs for regulatory factors. The Biochemical Journal 480, 957-974.

Broadley M, Brown P, Buerkert A, et al. 2012. Marschner's mineral nutrition of higher plants. San Diego: Academic Press.

Brodersen P, Sakvarelidze-Achard L, Schaller H, Khafif M, Schott G, Bendahmane A, Voinnet O. 2012. Isoprenoid biosynthesis is required for miRNA function and affects membrane association of ARGONAUTE1 in Arabidopsis. Proceedings of the National Academy of Sciences, USA 109, 1778-1783.

Buhtz A, Pieritz J, Springer F, Kehr J. 2010. Phloem small RNAs, nutrient stress responses, and systemic mobility. BMC Plant Biology 10, 64.

Carbonell A, Fahlgren N, Garcia-Ruiz H, Gilbert KB, Montgomery TA, Nguyen T, Cuperus JT, Carrington JC. 2012. Functional analysis of three Arabidopsis ARGONAUTEs using slicer-defective mutants. The Plant Cell **24**. 3613-3629.

Carbonell A, Carrington JC. 2015. Antiviral roles of plant ARGONAUTES. Current Opinion in Plant Biology 27, 111-117.

Carbonell A. 2017. Plant ARGONAUTEs: features, functions, and unknowns. Methods in Molecular Biology 1640, 1-21.

Chapman EJ, Carrington JC. 2007. Specialization and evolution of endogenous small RNA pathways. Nature Reviews. Genetics 8, 884-896.

Cisneros AE, de la Torre-Montaña A, Carbonell A. 2022. Systemic silencing of an endogenous plant gene by two classes of mobile 21-nucleotide artificial small RNAs. The Plant Journal 110, 1166-1181.

Cisneros AE, Martín-García T, Primc A, Kuziuta W, Sánchez-Vicente J, Aragonés V, Daròs J-A, Carbonell A. 2023. Transgene-free, virusbased gene silencing in plants by artificial microRNAs derived from minimal precursors. Nucleic Acids Research 51, 10719–10736.

Cisneros AE, Alarcia A, Llorens-Gámez JJ, Puertes A, Juárez-Molina M, Primc A, Carbonell A. 2025. Syn-tasiR-VIGS: virus-based targeted RNAi in plants by synthetic trans-acting small interfering RNAs derived from minimal precursors. Nucleic Acids Research 53, gkaf183.

Cui Y, Fang X, Qi Y. 2016. TRANSPORTIN1 promotes the association of microRNA with ARGONAUTE1 in Arabidopsis. The Plant Cell 28, 2576-2585.

Curtis MD, Grossniklaus U. 2003. A gateway cloning vector set for highthroughput functional analysis of genes in planta. Plant Physiology 133, 462-469

Derrien B, Baumberger N, Schepetilnikov M, Viotti C, De Cillia J, Ziegler-Graff V, Isono E, Schumacher K, Genschik P. 2012. Degradation of the antiviral component ARGONAUTE1 by the autophagy pathway. Proceedings of the National Academy of Sciences, USA 109, 15942-15946.

Ding Y, Ding L, Xia Y, Wang F, Zhu C. 2020. Emerging roles of microRNAs in plant heavy-metal tolerance and homeostasis. Journal of Agricultural and Food Chemistry 68, 1958-1965.

Dvořák P, Krasylenko Y, Ovečka M, Basheer J, Zapletalová V, Šamaj J, Takáč T. 2021. In vivo light-sheet microscopy resolves localisation patterns of FSD1, a superoxide dismutase with function in root development and osmoprotection. Plant, Cell & Environment 44, 68-87.

Earley K, Smith M, Weber R, Gregory B, Poethig R. 2010. An endogenous F-box protein regulates ARGONAUTE1 in Arabidopsis thaliana. Silence

Fang X, Qi Y. 2016. RNAi in plants: an argonaute-centered view. The Plant Cell 28, 272-285.

Farooq MA, Niazi AK, Akhtar J, Saifullah, Farooq M, Souri Z, Karimi N, Rengel Z. 2019. Acquiring control: the evolution of ROS-induced oxidative stress and redox signalling pathways in plant stress responses. Plant Physiology and Biochemistry 141, 353-369.

Gandikota M, Birkenbihl RP, Hohmann S, Cardon GH, Saedler H, Huiiser P. 2007. The miRNA156/157 recognition element in the 3' UTR of the Arabidopsis SBP-box gene SPL3 prevents early flowering by translational inhibition in seedlings. The Plant Journal 49, 683-693.

Garcia-Molina A, Andrés-Colás N, Perea-García A, Neumann U, Dodani SC, Huijser P, Peñarrubia L, Puig S. 2013. The Arabidopsis COPT6 transport protein functions in copper distribution under copperdeficient conditions. Plant and Cell Physiology 54, 1378-1390.

Guo AY, Zhu QH, Gu X, Ge S, Yang J, Luo J. 2008. Genome-wide identification and evolutionary analysis of the plant-specific SBP-box transcription-factor family. Gene 418, 1-8.

Gutierrez-Beltran E, Elander PH, Dalman K, Dayhoff GW, Moschou PN, Uversky VN, Crespo JL, Bozhkov PV. 2021. Tudor staphylococcal nuclease is a docking platform for stress-granule components and is essential for SnRK1 activation in Arabidopsis. The EMBO Journal 40, e105043.

Hacquard T, Clavel M, Baldrich P, et al. 2022. The Arabidopsis F-box protein FBW2 targets AGO1 for degradation to prevent spurious loading of illegitimate small RNA. Cell Reports 39, 110671.

Huijser P, Schmid M. 2011. The control of developmental phase transitions in plants. Development 138, 4117-4129.

Huntzinger E, Izaurralde E. 2011. Gene silencing by microRNAs: contributions of translational repression and mRNA decay. Nature Reviews. Genetics 12, 99-110.

Iki T, Yoshikawa M, Nishikiori M, Jaudal MC, Matsumoto-Yokoyama E, Mitsuhara I, Meshi T, Ishikawa M. 2010. In vitro assembly of plant RNA-induced silencing complexes facilitated by molecular chaperone HSP90. Molecular Cell 39, 282-291.

Iki T, Yoshikawa M, Meshi T, Ishikawa M. 2012. Cyclophilin 40 facilitates HSP90-mediated RISC assembly in plants. The EMBO Journal 31, 267-278

Iwasaki S, Kobayashi M, Yoda M, Sakaguchi Y, Katsuma S, Suzuki T, Tomari Y. 2010. Hsc70/Hsp90 chaperone machinery mediates ATP-dependent RISC loading of small-RNA duplexes. Molecular Cell 39,

Junglee S, Urban L, Sallanon H, Lopez-Lauri F. 2014. Optimised assay for hydrogen-peroxide determination in plant tissue using potassium iodide. American Journal of Analytical Chemistry 5, 730-736.

- Kim JJ, Lee JH, Kim W, Jung HS, Huijser P, Ahn JH. 2012. The microRNA156-SQUAMOSA PROMOTER BINDING PROTEIN-LIKE3 module regulates ambient-temperature-responsive flowering via FLOWERING LOCUS T in Arabidopsis. Plant Physiology 159, 461-478.
- Kobayashi T, Nozoye T, Nishizawa NK. 2019. Iron transport and its requlation in plants. Free Radical Biology & Medicine 133, 11-20.
- Kumar V, Pandita S, Singh Sidhu GP, Sharma A, Khanna K, Kaur P, Bali AS, Setia R. 2021. Copper bioavailability, uptake, toxicity and tolerance in plants: a comprehensive review. Chemosphere 262, 127810.
- Lamesch P, Berardini TZ, Li D, et al. 2012. The Arabidopsis information resource (TAIR): improved gene annotation and new tools. Nucleic Acids Research 40, D1202-D1210.
- Leung AKL, Calabrese JM, Sharp PA. 2006. Quantitative analysis of argonaute protein reveals microRNA-dependent localization to stress granules. Proceedings of the National Academy of Sciences, USA 103, 18125-18130.
- Liu C, Xin Y, Xu L, Cai Z, Xue Y, Liu Y, Xie D, Liu Y, Qi Y. 2018. Arabidopsis ARGONAUTE1 binds chromatin to promote gene transcription in response to hormones and stresses. Developmental Cell 44, 348–361.e7.
- Liu XM, Kim KE, Kim KC, et al. 2010. Cadmium activates Arabidopsis MPK3 and MPK6 via accumulation of reactive oxygen species. Phytochemistry 71, 614-618.
- Martin RC, Liu PP, Goloviznina NA, Nonogaki H. 2010. microRNA, seeds, and Darwin?: diverse function of miRNA in seed biology and plant responses to stress. Journal of Experimental Botany 61, 2229-2234.
- Martinez F, Rodrigo G, Aragones V, Ruiz M, Lodewijk I, Fernández U, Elena SF, Daròs J-A. 2016. Interaction network of tobacco etch potyvirus Nla protein with the host proteome during infection. BMC Genomics 17, 87.
- Martín-Merchán A, Lavatelli A, Engler C, González-Miguel VM, Moro B, Rosano GL, Bologna NG. 2024. Arabidopsis AGO1 N-terminal extension acts as an essential hub for PRMT5 interaction and post-translational modifications. Nucleic Acids Research 52, 8466-8482.
- Meister G. 2013. Argonaute proteins: functional insights and emerging roles. Nature Reviews. Genetics 14, 447-459.
- Melicher P, Dvořák P, Krasylenko Y, Shapiguzov A, Kangasjärvi J, Šamaj J, Takáč T. 2022. Arabidopsis iron superoxide dismutase FSD1 protects against methyl-viologen-induced oxidative stress in a copperdependent manner. Frontiers in Plant Science 13, 823561.
- Meng Y. Ma X. Chen D. Wu P. Chen M. 2010. MicroRNA-mediated signalling involved in plant root development. Biochemical and Biophysical Research Communications 393, 345-349.
- Molinier J. 2020. The multilayer's control of ARGONAUTE1 contents. Molecular Plant 13, 1-3.
- Morel JB, Godon C, Mourrain P, Béclin C, Boutet S, Feuerbach F, Proux F, Vaucheret H. 2002. Fertile hypomorphic ARGONAUTE (ago1) mutants impaired in post-transcriptional gene silencing and virus resistance. The Plant Cell 14, 629-639.
- Palatnik JF, Wollmann H, Schommer C, et al. 2007. Sequence and expression differences underlie functional specialization of Arabidopsis microRNAs miR159 and miR319. Developmental Cell 13, 115-125.
- Patel P, Yadav K, Ganapathi TR. 2017. Small and hungry: microRNAs in micronutrient homeostasis of plants. MicroRNA 6, 22-41.
- Pegler JL, Oultram JMJ, Nguyen DQ, Grof CPL, Eamens AL. 2021. MicroRNA-mediated responses to cadmium stress in Arabidopsis thaliana. Plants 10, 130
- Perea-García A, Andrés-Bordería A, Vera-Sirera F, Pérez-Amador MA, Puig S, Peñarrubia L. 2020. Deregulated high-affinity copper transport alters iron homeostasis in Arabidopsis. Frontiers in Plant Science 11, 1106.
- Perea-García A, Andrés-Bordería A, Huijser P, Peñarrubia L. 2021. The copper–microRNA pathway is integrated with developmental and environmental stress responses in Arabidopsis thaliana. International Journal of Molecular Sciences 22, 9547.

- Perea-García A, Puig S, Peñarrubia L. 2022. The role of posttranscriptional modulators of metalloproteins in response to metal deficiencies. Journal of Experimental Botany 73, 1735-1750.
- Perez-Riverol Y, Bai J, Bandla C, et al. 2022. The PRIDE database resources in 2022: a hub for mass-spectrometry-based proteomics evidences. Nucleic Acids Research 50, D543-D552.
- Perkins DN, Pappin DJC, Creasy DM, Cottrell John S. 1999. Probability-based protein identification by searching sequence databases using mass-spectrometry data. Electrophoresis 20, 3551–3567.
- Pilon M. 2011. Moving copper in plants. New Phytologist 192, 305–307.
- Pilon M. 2017. The copper microRNAs. New Phytologist 213, 1030–1035.
- Puig S, Peñarrubia L. 2009. Placing metal micronutrients in context: transport and distribution in plants. Current Opinion in Plant Biology 12, 299-306.
- Ravet K, Pilon M. 2013. Copper and iron homeostasis in plants: the challenges of oxidative stress. Antioxidants & Redox Signalling 19, 919-932.
- Rhoades MW, Reinhart BJ, Lim LP, Burge CB, Bartel B, Bartel DP. 2002. Prediction of plant microRNA targets. Cell 110, 513-520.
- Scarpeci TE, Zanor MI, Carrillo N, Mueller-Roeber B, Valle EM. 2008. Generation of superoxide anion in chloroplasts of Arabidopsis thaliana during active photosynthesis: a focus on rapidly induced genes. Plant Molecular Biology 66, 361-378.
- Schalk C, Cognat V, Graindorge S, Vincent T, Voinnet O, Molinier J. 2017. Small RNA-mediated repair of UV-induced DNA lesions by the DNA damage-binding protein 2 and ARGONAUTE1. Proceedings of the National Academy of Sciences, USA 114, 4734-4739.
- Schmidt TG, Batz L, Bonet L, Carl U, Holzapfel G, Kiem K, Matulewicz K, Niermeier D, Schuchardt I, Stanar K. 2013. Development of the twin-strep-tag® and its application for purification of recombinant proteins from cell-culture supernatants. Protein Expression and Purification 92,
- Schwab R, Palatnik JF, Riester M, Schommer C, Schmid M, Weigel D. 2005. Specific effects of microRNAs on the plant transcriptome. Developmental Cell 8, 517-527.
- Shahbaz M, Pilon M. 2019. Conserved Cu-microRNAs in Arabidopsis thaliana function in copper economy under deficiency. Plants 8, 141.
- Shilov IV, Seymour SL, Patel AA, Loboda A, Tang WH, Keating SP, Hunter CL, Nuwaysir LM, Schaeffer DA. 2007. The paragon algorithm, a next-generation search engine that uses sequence temperature values and feature probabilities to identify peptides from tandem mass spectra. Molecular & Cellular Proteomics 6. 1638-1655.
- Song X, Li Y, Cao X, Qi Y. 2019. MicroRNAs and their regulatory roles in plant-environment interactions. Annual Review of Plant Biology 70, 489-525.
- Sorin C, Declerck M, Christ A, et al. 2014. A miR169 isoform regulates specific NF-YA targets and root architecture in Arabidopsis. New Phytologist **202**, 1197–1211.
- Tomassi AH, Re DA, Romani F, Cambiagno DA, Gonzalo L, Moreno JE, Arce AL, Manavella PA. 2020. The intrinsically disordered protein CARP9 bridges HYL1 to AGO1 in the nucleus to promote microRNA activity. Plant Physiology **184**, 316–329.
- Trolet A, Baldrich P, Criqui M-C, et al. 2019. Cell-cycle-dependent regulation and function of ARGONAUTE1 in plants. The Plant Cell 31, 1734-1750.
- Vaucheret H, Vazquez F, Crete P, Bartel DP. 2004. The action of ARGONAUTE1 in the microRNA pathway and its regulation by the microRNA pathway are crucial for plant development. Genes & Development 18, 1187-1197.
- Vaucheret H, Mallory AC, Bartel DP. 2006. AGO1 homeostasis entails coexpression of MIR168 and AGO1 and preferential stabilization of miR168 by AGO1. Molecular Cell 22, 129-136.
- Wang W, Ye R, Xin Y, Fang X, Li C, Shi H, Zhou X, Qi Y. 2011. An importin-β protein negatively regulates microRNA activity in Arabidopsis. The Plant Cell 23, 3565-3576.

## 5480 | Tomassi et al.

**Waters BM, McInturf SA, Stein RJ**. 2012. Rosette iron-deficiency transcript and microRNA profiling reveals links between copper and iron homeostasis in *Arabidopsis thaliana*. Journal of Experimental Botany **63**, 5903–5918.

**Wu G, Poethig RS**. 2006. Temporal regulation of shoot development in *Arabidopsis thaliana* by miR156 and its target SPL3. Development **133**, 3539–3547.

**Wu M-F, Tian Q, Reed JW**. 2006. Arabidopsis microRNA167 controls patterns of ARF6 and ARF8 expression and regulates both female and male reproduction. Development **133**, 4211–4218.

Xing S, Salinas M, Höhmann S, Berndtgen R, Huijser P. 2010. miR156-targeted and nontargeted SBP-box transcription factors act in concert to secure male fertility in Arabidopsis. The Plant Cell 22, 3935–3950.

Yamasaki H, Abdel-Ghany SE, Cohu CM, Kobayashi Y, Shikanai T, Pilon M. 2007. Regulation of copper homeostasis by microRNA in Arabidopsis. Journal of Biological Chemistry 282, 16369–16378.

Yamasaki H, Hayashi M, Fukazawa M, Kobayashi Y, Shikanai T. 2009. SQUAMOSA promoter binding protein-like7 is a central regulator for copper homeostasis in Arabidopsis. The Plant Cell **21**, 347–361.